The Astrophysical Journal, 765:5 (8pp), 2013 March 1 doi:10.1088/0004-637X/765/1/5

PERIODIC VARIATIONS IN THE $O-C$ DIAGRAMS OF FIVE PULSATION FREQUENCIES OF THE DB WHITE DWARF EC 20058−5234*

J. Dalessio[1,2], D. J. Sullivan [3,7], J. L. Provencal[1,2], H. L. Shipman[1,2], T. Sullivan[3,7], D. Kilkenny[4], L. Fraga[5], and R. Sefako[6]

[1] Department of Physics and Astronomy, University of Delaware, Newark, DE 19716, USA
[2] The Delaware Asteroseismology Research Center, DE, USA
[3] School of Chemical & Physical Sciences, Victoria University of Wellington, P.O. Box 600, Wellington 6012, New Zealand
[4] Department of Physics, University of the Western Cape, Private Bag X17, Bellville 7535, South Africa
[5] Southern Observatory for Astrophysical Research, Casilla 603, La Serena, Chile
[6] South African Astronomical Observatory, P.O. Box 9, Observatory 7935, South Africa
Received 2012 October 18; accepted 2012 December 19; published 2013 February 8

ABSTRACT

Variations in the pulsation arrival time of five independent pulsation frequencies of the DB white dwarf EC 20058−5234 individually imitate the effects of reflex motion induced by a planet or companion but are inconsistent when considered in unison. The pulsation frequencies vary periodically in a 12.9 year cycle and undergo secular changes that are inconsistent with simple neutrino plus photon-cooling models. The magnitude of the periodic and secular variations increases with the period of the pulsations, possibly hinting that the corresponding physical mechanism is located near the surface of the star. The phase of the periodic variations appears coupled to the sign of the secular variations. The standards for pulsation-timing-based detection of planetary companions around pulsating white dwarfs, and possibly other variables such as subdwarf B stars, should be re-evaluated. The physical mechanism responsible for this surprising result may involve a redistribution of angular momentum or a magnetic cycle. Additionally, variations in a supposed combination frequency are shown to match the sum of the variations of the parent frequencies to remarkable precision, an expected but unprecedented confirmation of theoretical predictions.

Key words: asteroseismology – planets and satellites: detection – stars: oscillations – stars: variables: general – subdwarfs – white dwarfs

Online-only material: color figures

1. INTRODUCTION AND FORMALISM

The orbital motion of a planet hosting star about the system's mass center, often referred to as a "wobble," will cause variations in the time it takes for light from the star to reach external observers. If the star provides some predictable repetitive behavior, like regular pulsations, the wobble will cause systematic differences between the time the behavior is predicted to be observed and when it is actually observed. This phenomenon has resulted in the discovery of the first known exoplanet and the rest of the pulsar planets (Wolszczan & Frail 1992; Thorsett et al. 1993), confirmation and detection of a growing number of planets with *Kepler* transit timing variations (see Holman et al. 2010 and subsequent *Kepler* publications), a planet around a subdwarf B star (Silvotti et al. 2007), as well as strong detection limits on several pulsating white dwarfs (Mullally et al. 2008; Hermes et al. 2010) and one tentative white dwarf planet candidate (Mullally et al. 2009). However, changes to the actual frequency of the repetitive behavior will also manifest as differences between the expected and actual time the behavior is observed. To illustrate this, imagine observations of two distant ticking clocks. Clock one keeps poor time. Everyday the period of the ticks changes in such a way that clock one appears a second slow at noon and a second fast at midnight. Clock two keeps perfect time but is moving in a light second orbit in the plane of the observer with a period of a day. While these clocks are fundamentally very different, the two clocks are indistinguishable in terms of timing alone. It has been asserted via lex parsimoniae (Occam's Razor), specifically for white dwarf pulsators, that any sinusoidal or "planet-like" variations in the timing of the pulsations are most likely due to orbital motion as there is no known mechanism that would conspire to make the actual pulsation frequency vary in such a manner. This paper presents conclusive evidence to the contrary: frequency variations in a white dwarf pulsator that can mimic the effect of a planetary companion.

The dominant cooling mechanism for the hot pulsating DB white dwarfs is thought to be the production of plasmon neutrinos. The frequency of the pulsations is determined in part by the temperature, so cooling should cause a slow secular change in frequency. This effect has been well studied with the far cooler, photon-cooling-dominated DA white dwarf G117-B15A (Kepler et al. 2005). If the rate of frequency change of a hot pulsating DB white dwarf was measured to sufficient precision, the neutrino production rate could be extracted and used to constrain the Standard Model (Winget et al. 2004). This paper presents evidence that there are other processes that cause large secular changes to multiple pulsation frequencies in a white dwarf.

The diagnostic tool used to measure variations in pulsation arrival time and pulsation frequency is called the $O-C$, or "observed minus calculated" diagram. Depending on the implementation, "observed minus calculated" can be a misnomer. In many cases it is a plot of successive measurements of the

* Based on observations obtained at the Southern Astrophysical Research (SOAR) telescope, which is a joint project of the Ministério da Ciência, Tecnologia, e Inovação (MCTI) da República Federativa do Brasil, the US National Optical Astronomy Observatory (NOAO), the University of North Carolina at Chapel Hill (UNC), and Michigan State University (MSU).
[7] Visiting astronomer, Mt. John University Observatory, operated by the Department of Physics & Astronomy, University of Canterbury.

Table 1
Journal of Observations and Binning Scheme

Observatory	Date Range	Instrument	Observations
SAAO	1994 May 14–1994 Jun 2	PMT	5535
SAAO	1994 Jul 6–1994 Jul 12	PMT	6881
SAAO	1994 Oct 3–1994 Oct 3	PMT	1304
SAAO	1994 Jun 12–1994 Jun 12	PMT	1378
XCOV15	1997 Jul 2–1997 Jul 11	PMT	46,289
Mt. John	1997 Oct 5–1997 Oct 6	PMT	3162
Mt. John	1998 Jul 24–1998 Jul 25	PMT	7057
Mt. John	1998 Aug 14–1998 Aug 14	CCD	1153
Mt. John	1999 Sep 9–1999 Sep 13	PMT	1517
Mt. John	2000 Jul 6–2000 Jul 8	PMT	8025
Mt. John	2000 Sep 5–2000 Sep 5	PMT	770
Mt. John	2001 Mar 30–2001 Apr 1	PMT	2101
Mt. John	2001 Sep 21–2001 Sep 24	PMT	7710
Mt. John	2002 Apr 12–2002 Apr 15	PMT	8872
Mt. John	2002 Aug 1–2002 Aug 6	PMT	12,672
Mt. John	2002 Sep 5–2002 Sep 9	PMT	3814
Magellan	2003 Jul 11–2003 Jul 13	CCD	2317
Magellan	2003 Jul 25–2003 Jul 31	CCD	8865
Mt. John	2003 Aug 27–2003 Sep 2	PMT	12,216
Mt. John	2003 Sep 22–2003 Sep 23	PMT	4694
Mt. John	2003 Oct 31–2003 Oct 31	PMT	1229
Mt. John	2004 Apr 23–2004 Apr 25	PMT	2474
Mt. John	2004 May 16–2004 May 16	PMT	1599
Mt. John	2004 Jun 9–2004 Jun 16	PMT	14,554
Mt. John	2004 Jul 9–2004 Jul 14	PMT	17,240
Mt. John	2004 Aug 7–2004 Aug 10	PMT	5072
CTIO SMARTS	2004 Aug 24–2004 Aug 28	CCD	2320
CTIO SMARTS	2005 Sep 21–2005 Sep 25	CCD	979
CTIO SMARTS	2006 Aug 31–2006 Sep 13	CCD	5019
CTIO SMARTS	2007 Aug 17–2007 Sep 6	CCD	14,117
Mt. John	2007 Jul 16–2007 Jul 17	PMT	6281
CTIO SMARTS	2008 Aug 29–2008 Sep 1	CCD	1736
Mt. John	2008 Aug 30–2008 Aug 31	CCD	3092
XCOV27[a]	2009 May 18–2009 May 26	CCD	4609
Mt. John	2010 Jul 5–2010 Jul 11	CCD	20,201
CTIO SMARTS	2011 Sep 8–2011 Sep 15	CCD	3584

Notes. Note that only the light curves from XCOV15 and XCOV27 consist of data from multiple sites.
[a] XCOV27 included observations from SOAR, SAAO, and the CTIO SMARTS 36.

absolute phase of a periodic variation assuming constant frequency. The ordinate and abscissa of the $O-C$ diagram are both expressed in units of time, but are sometimes normalized by the typical period of the behavior into units of cycles (often labeled "epochs" on the abscissa), radians, or degrees. The $O-C$ diagram can reveal frequency changes that are difficult to detect by direct measurement. In addition to the detection of planets around pulsars and other pulsating stars, it was the primary diagnostic tool that helped earn Hulse and Taylor the Nobel Prize in Physics for their indirect detection of gravitational wave emission (Taylor et al. 1979). The $O-C$ diagram remains a critical tool across time domain astronomy (see, e.g., Oksala et al. 2012; Barlow et al. 2011; Mullally et al. 2008; Hermes et al. 2012).

For pulsating white dwarf stars and other short-period variables, it is convenient to describe $O-C$ as a time-varying absolute phase. Given some fixed observed frequency, $f_{\rm obs}$, the instantaneous amplitude of a pulsation can be rewritten in terms of the time-varying absolute phase, $\tau(t)$,

$$H(t) = A\sin(2\pi f_{\rm obs}(t-\tau(t))), \quad (1)$$

$\tau(t)$ can be mathematically described as (for a complete derivation, see Dalessio et al. 2012)

$$\tau(t) = t_0 - \frac{\delta f_{\rm obs}}{f_{\rm obs}}t - \frac{1}{f_{\rm obs}}\int^t \gamma(t')dt' + \frac{q(t)}{c}, \quad (2)$$

where t_0 is an arbitrary offset depending on choice of $t=0$, $f_{\rm obs}$ is the observed frequency, $\delta f_{\rm obs}$ is the difference between the observed and actual, time-averaged, Doppler shifted frequency, $\gamma(t)$ is the perturbation to the frequency, and $q(t)$ is the perturbation to the distance between the object and observer. Note that $\gamma(0)=q(0)=0$.

Except in the case of continuous observation where the number of elapsed cycles is explicitly known, all points in the $O-C$ diagram suffer from the ambiguity that they can be shifted up or down by any integer times the pulsation period. A common assumption is that $O-C$ has been sampled often enough that $\gamma(t)$ and $q(t)$ change slowly and smoothly during the observational gaps. Under this assumption, the location of the points on an $O-C$ diagram can be constrained if there is a single unambiguous configuration that creates a smooth, continuous trend.

2. OBSERVATIONS

EC 20058−5234 (Koen et al. 1995) has been identified as a prime candidate for measurement of the neutrino production rate in a white dwarf (see Section 1). This motivated many of the over 250,000 PMT (photo-multiplier tube) and CCD (charge-coupled device) photometric measurements spanning 1994–2011. EC 20058−5234 was a primary target of the Whole Earth Telescope campaign XCOV15 in 1997 (Sullivan et al. 2008), followed by seasonal high-speed photometry from the 1 m McLellan telescope at Mt. John Observatory and the 36 inch SMARTS telescope at CTIO (see, e.g., Sullivan 2005). It was also a tertiary target during XCOV27 and was observed at Magellan in 2003 (Sullivan et al. 2007). A summary of the observations is shown in Table 1.

3. RESULTS AND ANALYSIS

3.1. Data Reduction and Preparation

The PMT photometry obtained at SAAO in 1994 was reduced as described in Koen et al. (1995), while the 1997 XCOV15 photometry and the Mt. John PMT photometry was reduced using the methods outlined in Sullivan et al. (2008). All the Mt. John PMT photometry collected between 1998 July and 2007 July employed a three-channel photometer (Sullivan 2000) attached to the 1 m McLellan telescope. All CCD image calibration and aperture photometry were performed with Maestro (Dalessio 2010). WQED (Thompson & Mullally 2009) was used to remove spurious points and to perform the barycentric correction (for a review see Eastman et al. 2010) for the CCD data. The barycentric correction applied to the PMT data was performed using the same implementation as used in WQED (Stumpff 1980). The photometric measurements were divided into 36 individual light curves, one for each observing campaign in Table 1. The following analysis was also performed by dividing the points into light curves for each individual night and observing season. The differences were not significant and do not merit further discussion.

3.2. Testing for Stability

The frequency and amplitude of all pulsation frequencies with amplitudes above 0.1% were extracted from two of the

Table 2
Pulsation Frequencies with Amplitudes Above 0.1% as Directly Measured from XCOV15 and the 2007 CTIO SMARTS Data Sets

Label	Period (s)	Frequency (μHz)		Amplitude (mma)		
	(approx)	1997	2007	1997	2007	Ratio
A	134	7452.18(.05)	7452.27(.02)	1.67	2.2	1.3(.1)
B	195	5128.53(.03)	5128.71(.02)	2.51	3.3	1.31(.09)
C	204	4902.14(.05)	4902.14(.02)	1.47	2.6	1.8(.2)
D	205	4887.84(.03)	4887.91(.02)	2.62	3.2	1.22(.09)
E	257	3893.142(.009)	3893.239(.005)	8.37	11.3	1.35(.03)
F	275	3640.37(.07)		1.13		
G	281	3559.032(.009)	3559.033(.005)	8.45	10.5	1.24(.03)
H	287	3489.07(.05)	3489.05(.02)	1.58	2.2	1.4(.1)
I	333	2998.67(.03)	2998.71(.01)	3.01	4.3	1.43(.08)
J	350	2852.36(.09)		1.40		
K	525	1903.61(.04)	1903.49(.02)	1.83	2.44	1.3(.1)
L	540	1852.53(.04)		1.86		

Notes. The standard error in the measurement of the amplitude of all frequencies was 0.09 mma (1 mma = 0.1%) in the 2007 CTIO SMARTS data set and 0.2 mma in the XCOV15 data set. Several frequencies from XCOV15 were not detected in the 2007 data set but would have been had the amplitude remained constant. The systematic increase in amplitude from 1997 to 2007 is an observational artifact. The transition from PMTs to CCD imaging now allows removal of some of the flux of the nearby companions. The ratio of pulsation amplitudes from 2007 to 1997 is consistent with having a constant amplitude with a reduced χ^2 value of 2.3 and a likelihood of around 10%.

largest data sets, XCOV15 in 1997 and the 2007 CTIO SMARTS observations. The results are summarized in Table 2. The same spectrum of frequencies appears in both years (see the Fourier spectrum from Sullivan et al. 2008), with the exception that pulsation frequencies F, J, and L have amplitudes below the noise threshold in 2007 and that pulsation frequency E appears to have changed at a statistically significant level. The systematically higher pulsation amplitudes in 2007 are an observational effect due to two companions within several arcseconds of EC 20058−5234 (see the figure in Koen et al. 1995). The PMT observations included all three objects as it was impractical in the typically 2″ seeing conditions at Mt. John to separate flux from the target only. However, the CCD data, especially when combined with the better seeing conditions at CTIO and the Magellan site, permitted extraction of just the flux from EC 20058−5234 using synthetic aperture techniques. This effect makes it non-trivial to search for amplitude modulation, which, particularly for RR Lyrae stars, is known to be coupled to phase modulation (the Blazhko effect; see, e.g., Buchler & Kolláth 2011). However, if the pulsation amplitudes are intrinsically constant, the ratio of amplitudes from one set to another should be constant. The ratio of the pulsation amplitudes from 2007 to the pulsation amplitudes in 1997 is shown in the last column of Table 2. The ratio is consistent with there being no amplitude variation with a reduced χ^2 value of 2.3 with a statistical likelihood around 10%. This is the worst reduced χ^2 value for the model of constant amplitude between any two of the data sets in Table 1. This value of reduced χ^2 is slightly higher than expected for a constant amplitude. The removal of atmospheric extinction and other observational effects could introduce small changes in observed amplitude so we do not find this slight disagreement particularly alarming. Even if the amplitude of these pulsations frequencies is intrinsically changing, the changes are relatively small and only barely distinguishable between our two best data sets.

Table 3
Precision of Frequency Measurements from Bootstrapping of Data from 2003 September to 2004 August

Label	Period (s)	Frequency (μHz)	$1/\sigma_f$ (yr)
A	134	7452.249(.001)	32
B	195	5128.598(.001)	32
C	204	4902.176(.0009)	35
D	205	4887.8491(.0009)	35
E	257	3893.2482(.0002)	160
G	281	3559.0017(.0003)	106
H	287	3489.056(.001)	29
I	333	2998.7144(.0007)	45
J	350	2852.439(.002)	19
K	525	1903.464(.001)	24

Note. Standard errors are quoted in parentheses.

3.3. Extracting Precise Frequencies

Precise measurements of the pulsation frequencies were made using the "bootstrapping" procedure. The process is described as follows. The frequencies above the noise threshold in the 2004 July data set were extracted. A sum of sinusoids (one sinusoid at each frequency) were fit to the 2004 July data set using nonlinear least squares and allowing each frequency to converge to the optimum value. After the fit converged, additional data were added to the set, ensuring that each of the frequencies had been measured to sufficient precision so that if the frequency had remained constant, there would be no ambiguity in the number of cycles between any two data points in the combined set. This ensures that the linear term of Equation (2) will not dominate the $O-C$ diagram and that the frequencies are clearly separated from the aliases of the combined set. After the new data were added, the frequencies were refitted. This process was repeated until most of the 2003 and 2004 data were combined into a single set. The amplitudes of pulsation frequencies F and L were well below the noise threshold and were not considered. The combined set of all data between 2003 September and 2004 August gave precise enough frequency measurements to merge the entire data set. However, merging the September 2003–August 2004 data set with data from August 2003 or 2005 decreased the precision of our frequency measurements. This is an indication that the phase/frequency of the pulsation frequencies is changing by a substantial amount over that time span. Further combination was abandoned beyond the 2003 September–2004 August pulsation frequency measurements. The results are summarized in Table 3.

3.4. Building the $O-C$ Diagrams

A sum of sinusoids at the 10 frequencies in Table 3 were linearly fit to each data set. The calculated absolute phase was plotted as $O-C$ for each pulsation frequency. The $O-C$ diagram of all 10 pulsation frequencies showed structure that was not consistent with scatter. It was also apparent that for some frequencies, $O-C$ was changing by a large fraction of the period, and that *none* of the $O-C$ diagrams were consistent with the parabolic trend of a simple neutrino plus photon-cooling model (Bischoff-Kim 2008).

It was assumed (see Section 1) that for each pulsation frequency, $\gamma(t)$ and $q(t)$ change slowly and smoothly during the observational gaps. An unambiguous smooth trend in the $O-C$ diagrams of pulsation frequencies A, D, E, G, H, and I

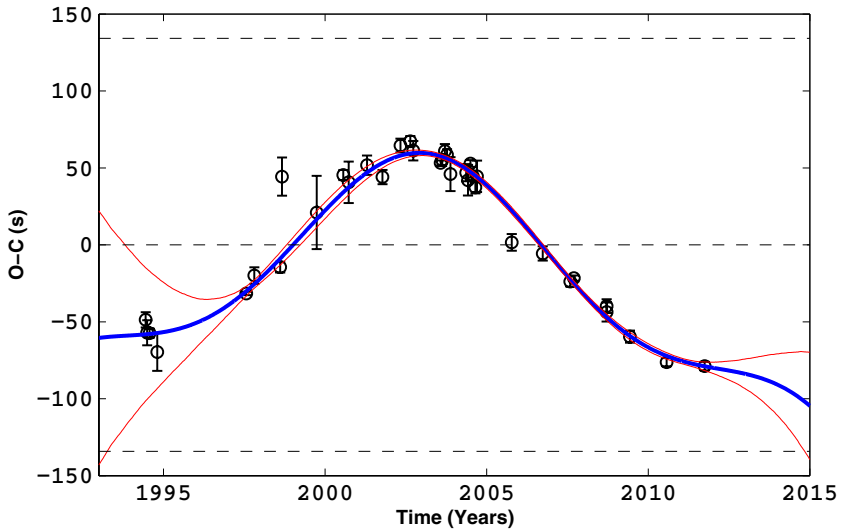

Figure 1. $O-C$ of pulsation frequency A. The dashed lines are located at 0, P, and $-P$. The blue line is the best model fit for $\Pi = 12.9$ years. The red lines indicate the boundaries of the 1σ likelihood prediction of the model not including the 1994 data. Note that a first-order polynomial has been removed from the data.
(A color version of this figure is available in the online journal.)

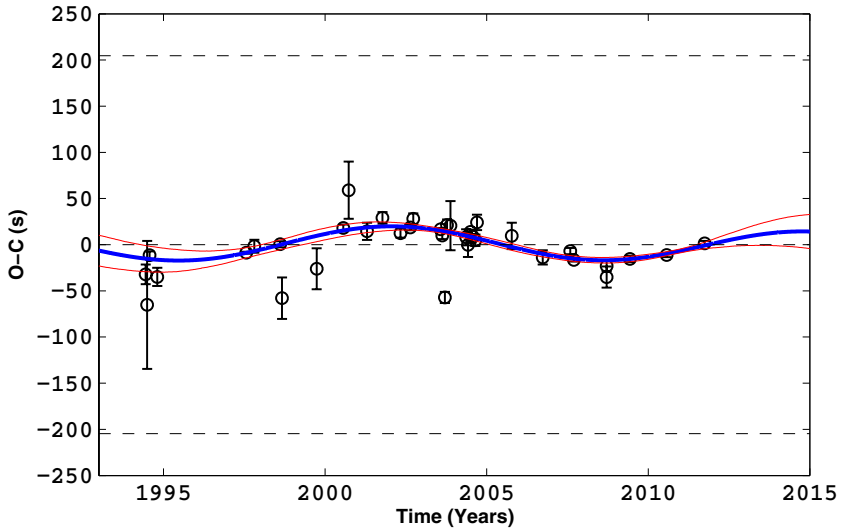

Figure 2. $O-C$ of pulsation frequency D. The dashed lines are located at 0, P, and $-P$. The blue line is the best model fit for $\Pi = 12.9$ years. The red lines indicate the boundaries of the 1σ likelihood prediction of the model not including the 1994 data. Note that a first-order polynomial has been removed from the data.
(A color version of this figure is available in the online journal.)

was clearly discernible and the $O-C$ measurements were fixed to an appropriate location on the $O-C$ diagram. Due to the large observational gap between 1994 and 1997, the measurements from 1994 remained unconstrained. The appropriate location in the $O-C$ diagram of the 1994 $O-C$ measurements is further addressed in Section 3.5. No unambiguous trend was apparent in the $O-C$ diagrams of pulsation frequencies C, B, J, and K and they were removed from analysis. The $O-C$ diagrams of pulsation frequencies A, D, E, G, H, and I are shown in Figures 1–6.

3.5. Modeling the $O-C$ Variations

All six $O-C$ diagrams (Figures 1–6) show some sort of oscillatory behavior. A sinusoid plus an offset, linear, and parabolic term were chosen as a suitable model. The model is mathematically described as

$$\tau(t) = t_0 - \frac{\delta f_{\rm obs}}{f_{\rm obs}} t + \frac{\dot{P}}{2P_{\rm obs}} t^2 + \frac{\alpha \Pi}{2\pi f_{\rm obs}} \sin\left(\frac{2\pi}{\Pi} t - \phi\right). \quad (3)$$

Instead of fitting this nonlinear model with some initial guesses to t_0, $\delta f_{\rm obs}$, the rate of period change $\dot{P}$, the amplitude of the sinusoidal frequency variation α, the period of the sinusoidal frequency variation Π, and the absolute phase of the sinusoidal frequency variation ϕ, a grid of linear fits can be calculated for a range of Π. By removing any dependence on initial guesses for the parameters, it is guaranteed that the absolute minimum in χ^2 over the chosen range of Π will be found. A Monte Carlo simulation was performed to calculate the statistical likelihood of the possible locations of the 1994 measurements given the model and the 1997–2012 measurements. The 1σ likelihood boundaries are indicated in Figures 1–6. It was concluded that for all frequencies there was only one reasonable choice for the possible values of the 1994 $O-C$ measurements and that all ambiguity could be considered resolved for the given model. The 1994 $O-C$ measurements were then fixed to these values in each $O-C$ diagram. Fits to Equation (3) were then calculated over a range of Π for each of the $O-C$ diagrams. A plot of the reduced χ^2 for the fit of each of the six $O-C$ diagrams as

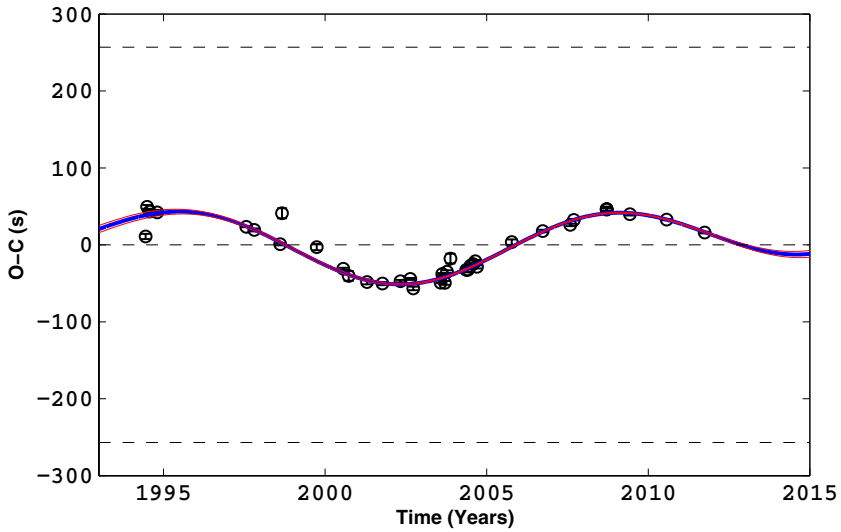

Figure 3. $O-C$ of pulsation frequency E. The dashed lines are located at 0, P, and $-P$. The blue line is the best model fit for $\Pi = 12.9$ years. The red lines indicate the boundaries of the 1σ likelihood prediction of the model not including the 1994 data. Note that a first-order polynomial has been removed from the data.
(A color version of this figure is available in the online journal.)

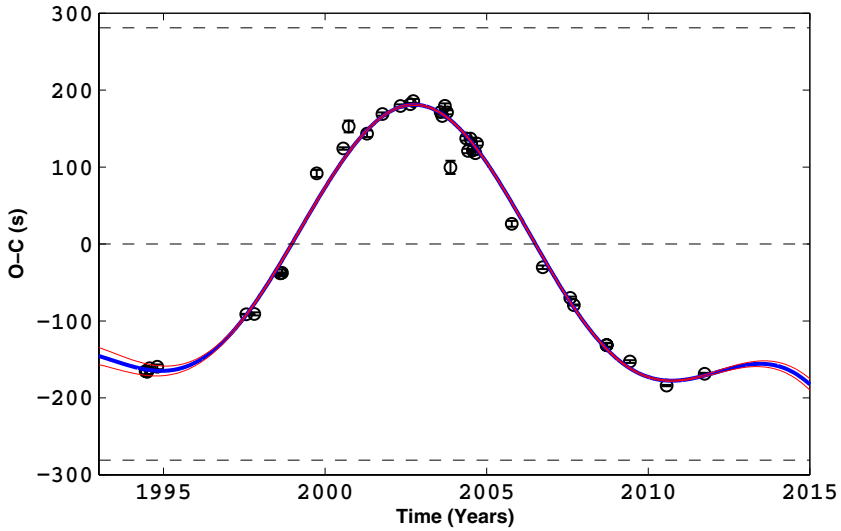

Figure 4. $O-C$ of pulsation frequency G. The dashed lines are located at 0, P, and $-P$. The blue line is the best model fit for $\Pi = 12.9$ years. The red lines indicate the boundaries of the 1σ likelihood prediction of the model not including the 1994 data. Note that a first-order polynomial has been removed from the data.
(A color version of this figure is available in the online journal.)

a function of Π is shown in Figure 7. Four of the six $O-C$ diagrams have a strong periodicity at around 13 years, while the other two are not particularly sensitive to the choice of period, but are consistent with a periodicity of 13 years. The minima of the total reduced χ^2 for all six $O-C$ diagrams are at $\Pi = 12.9$ years. This value of Π was used to fit each $O-C$ diagram. The best fits are overlayed in Figures 1–6 and Table 4 summarizes the resultant parameters. The large value of the reduced χ^2 for some of the fits is disturbing, but the ability of the model to reproduce the *overall* trend in the data is excellent. To further investigate, Π was then allowed to vary for each individual $O-C$. This leads to a worse overall reduced χ^2, an indicator that the oscillatory behavior in each $O-C$ is represented appropriately by the same Π. Fitting the data with high-order polynomials did not result in a dramatic improvement in reduced χ^2. An eighth-order polynomial, for example, actually increased the reduced χ^2 for two of the $O-C$ diagrams and only led to an overall improvement of 7% over Equation (3). Equation (3) is dramatically more constrained than a polynomial with a similar number of degrees of freedom so this strongly supports the ability of Equation (3) to represent the overall trends in the data. The high values of the reduced

Table 4
Resultant Fit Parameters from Fitting Equation (3) to the Six $O-C$ Diagrams

Label	Period (s)	$\dot{P}$ (10^{-14})	α ($10^{-9}\frac{1}{s}$)	Φ (deg)	$\chi^2_{\rm Red}$
A	134	−28(1)	4.0(.1)	160(2)	3.3
D	205	−1(2)	1.33(.09)	187(4)	6.6
E	257	13.0(.8)	2.48(.02)	0(1)	14
G	281	−131(1)	6.44(.03)	166.6(.2)	26
H	287	88(6)	6.8(.1)	1(1)	2.8
I	333	313(4)	7.31(.07)	−1(1)	13

Note. Note the high values of the reduced χ^2 fit mean that some of the formal quoted errors are unreliable, even though the model reproduces the overall trends in the data very well.

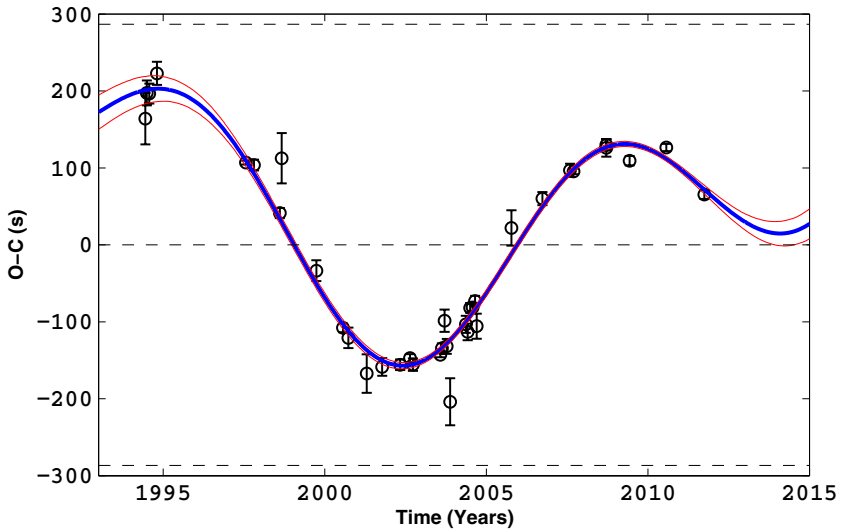

Figure 5. $O-C$ of pulsation frequency H. The dashed lines are located at 0, P, and $-P$. The blue line is the best model fit for $\Pi = 12.9$ years. The red lines indicate the boundaries of the 1σ likelihood prediction of the model not including the 1994 data. Note that a first-order polynomial has been removed from the data.
(A color version of this figure is available in the online journal.)

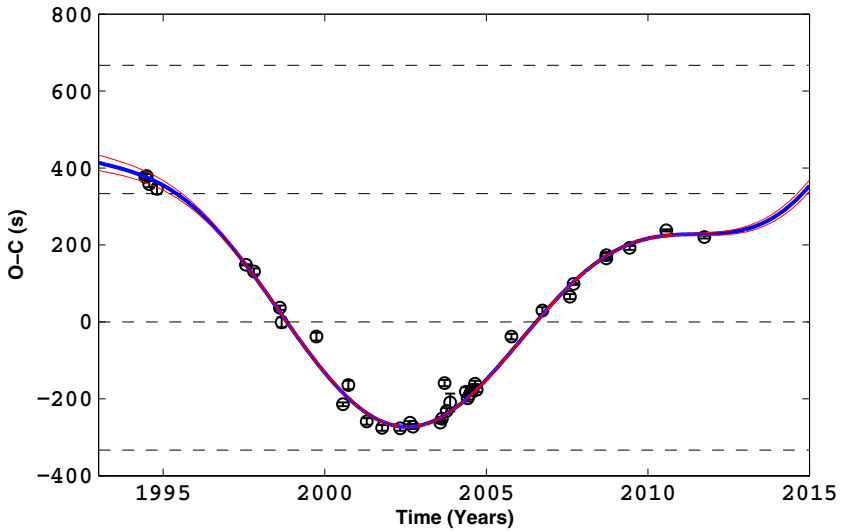

Figure 6. $O-C$ of pulsation frequency I. The dashed lines are located at 0, P, $-P$, and $2P$. The blue line is the best model fit for $\Pi = 12.9$ years. The red lines indicate the boundaries of the 1σ likelihood prediction of the model not including the 1994 data. Note that a first-order polynomial has been removed from the data.
(A color version of this figure is available in the online journal.)

χ^2 mean that either the error bars in the data are somehow underestimated or there are high-frequency variations in $O-C$ that are undersampled. To investigate, the Fourier transforms of the averaged residuals and absolute averaged residuals (see Figure 8) were calculated. There was no statistically significant or notable power at any frequency, although the residuals appear correlated. It is concluded that there are likely unresolved variations in phase, but these variations do not dilute the effectiveness of Equation (3) in modeling the overall variations.

4. DISCUSSION

4.1. Planetary Detection with the Pulsation Timing Method

The sinusoidal component of the variations shown in Figures 1–6 do not share the same amplitude and phase, so are clearly not due to the effects of a planetary companion. Had only one of the pulsation frequencies in this star been analyzed, this paper could very well be announcing the first detection of a planet around a white dwarf. The discovery that multiple $O-C$ diagrams can show similar periodic behavior when not in the presence of a planetary companion is alarming. Pulsation-timing-based white dwarf planet detection should now require supplemental confirmation, even when similar pulsation timing variations are observed in multiple pulsation frequencies. Until the physical mechanisms behind these variations are identified as specific to white dwarfs, these observations cast at least some shadow of doubt on the effectiveness of pulsation timing to *reliably* detect planetary companions to subdwarf B pulsators, and raise at least some skepticism as to the existence the subdwarf B planet V391 Pegasi b. We note that this does not affect the ability of the pulsation timing method to *exclude* the existence of planets around white dwarfs and other variables. The lack of known white dwarf planets is gaining statistical significance and further timing observations of pulsating white dwarfs could place strong constraints on post-main-sequence stellar evolution.

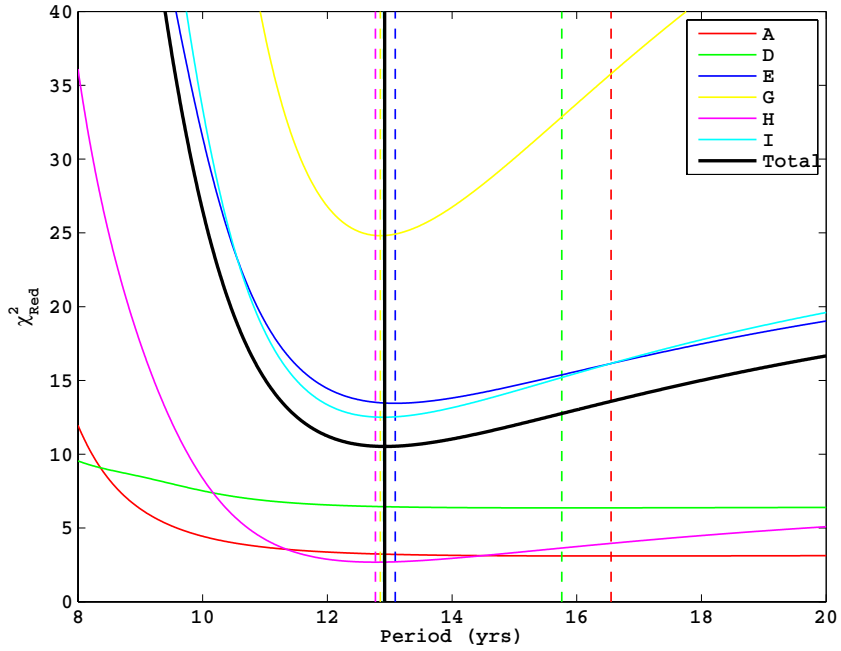

Figure 7. Reduced χ^2 as a function of Π (see Equation (3)) for each of the coherent $O-C$ diagrams. The average minimum is at 12.9 years.
(A color version of this figure is available in the online journal.)

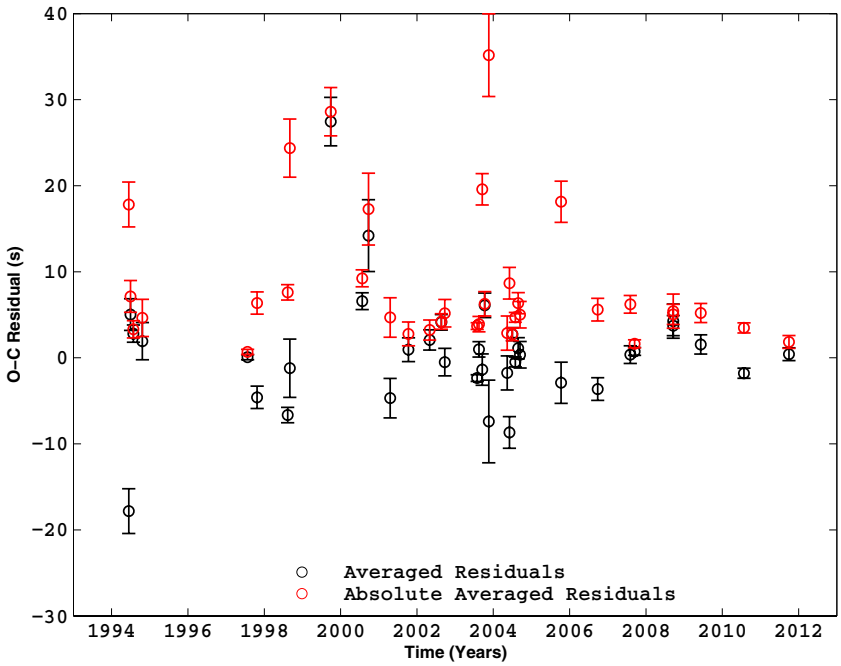

Figure 8. Residuals of the fit of Equation (3) to the $O-C$ diagrams of D, E, G, H, and I. The black points are the weighted average residuals for each data set, while the red points are the weighted average of the absolute value of the residuals.
(A color version of this figure is available in the online journal.)

4.2. The Combination Frequency A

Sullivan et al. (2008) identified the frequency of A to be an additive combination of the frequencies of E and G, a well-known occurrence in white dwarf pulsators (see, e.g., Provencal et al. 2009). Any perturbation to the frequency of E or G should result in an identical perturbation to the frequency of A. The frequency perturbations found by fitting Equation (3) to the $O-C$ diagram of E, G, and A can be compared, see Table 5. The agreement is outstanding. This is

Table 5
Comparison of the Modeled Variations of the Combination Frequency A to Its Parents E and G

Parameter	A	E + G
$\dot{f} = -\frac{\dot{P}}{P^2}$ $(\frac{10^{-18}}{s^2})$	14.6(.2)	15.3(.5)
α $(\frac{10^{-9}}{s})$	4.0(.1)	4.07(.03)
ϕ (deg)	160(2)	158.7(.2)

strong evidence that Equation (3) is effectively modeling the frequency perturbations and that the parabolic and sinusoidal components of the perturbation are linearly independent. It is also the most conclusive evidence that combination frequencies are indeed exactly equal to the additive frequency of the parents as predicted by Wu (2001).

4.3. An Asteroseismologic Interpretation of the Results

The frequency of these pulsations is dependent on many physical quantities, including the star's rotational velocity, magnetic field strength, and magnetic field geometry (for an in-depth review, see Unno et al. 1979). Any redistribution of angular momentum or change in magnetic field strength (or geometry) would change the observed frequencies. The sign of the first-order frequency perturbation caused by changes in rotation is well known to depend solely on whether the pulsations are moving with or against rotation. In other words, if one pulsation is moving with rotation and another against it, a redistribution of angular momentum would perturb the frequency of the two pulsations in the opposite direction. The variations in pulsation frequencies E, H, and I have positive $\dot{P}$ and $\phi \approx 0^\circ$, while pulsation frequencies D and G have negative $\dot{P}$ and ϕ close to 180°. We speculate that one of these groups of pulsation frequencies could be moving with rotation and the other against rotation and that the observed variations in $O-C$ may be caused by changes in the star's rotation profile. Additionally, the long-period g-mode pulsation frequencies in white dwarfs are well known to be more affected by physical properties at the surface of the star than short-period g-mode pulsation frequencies. The observed frequency perturbations appear to affect the longer period pulsations more, a hint that the corresponding physical processes responsible for these frequency variations may be near the surface of the star. We again emphasize the speculative nature of these interpretations. The possible effects of magnetic field variations and quantitative modeling of these frequency variations will be investigated in the primary author's doctoral dissertation.

J.D., J.L.P., and H.L.S. thank the Crystal Trust for supporting this research. J.D. thanks the Delaware Space Grant Consortium for financial support. D.J.S. and T.S. thank the Department of Physics and Astronomy at the University of Canterbury for the generous allocation of telescope time for this project and the VUW Faculty of Science for financial assistance. D.K. thanks the University of the Western Cape and the South African Foundation for Research Development (FRD) for continuing financial support. This paper uses observations made at the South African Astronomical Observatory (SAAO).

REFERENCES

Barlow, B. N., Dunlap, B. H., Clemens, J. C., et al. 2011, MNRAS, 414, 3434
Bischoff-Kim, A. 2008, CoAst, 154, 16
Buchler, J. R., & Kolláth, Z. 2011, ApJ, 731, 24
Dalessio, J. 2010, BAAS, 42, 215
Dalessio, J., Provencal, J. L., Barlow, B. N., & Shipman, H. L. 2012, in Proc. 18th European White Dwarf Workshop, submitted
Eastman, J., Siverd, R., & Gaudi, B. S. 2010, PASP, 122, 935
Hermes, J. J., Kilic, M., Brown, W. R., et al. 2012, ApJL, 757, L21
Hermes, J. J., Mullally, F., Winget, D. E., et al. 2010, in AIP Conf. Proc., 1273, 17th European White Dwarf Workshop, ed. K. Werner & T. Rauch (Melville, NY: AIP), 446
Holman, M. J., Fabrycky, D. C., Ragozzine, D., et al. 2010, Sci, 330, 51
Kepler, S. O., Costa, J. E. S., Castanheira, B. G., et al. 2005, ApJ, 634, 1311
Koen, C., O'Donoghue, D., Stobie, R. S., Kilkenny, D., & Ashley, R. 1995, MNRAS, 277, 913
Mullally, F., Reach, W. T., De Gennaro, S., & Burrows, A. 2009, ApJ, 694, 327
Mullally, F., Winget, D. E., De Gennaro, S., et al. 2008, ApJ, 676, 573
Oksala, M. E., Wade, G. A., Townsend, R. H. D., et al. 2012, MNRAS, 419, 959
Provencal, J. L., Montgomery, M. H., Kanaan, A., et al. 2009, ApJ, 693, 564
Silvotti, R., Schuh, S., Janulis, R., et al. 2007, Natur, 449, 189
Stumpff, P. 1980, A&AS, 41, 1
Sullivan, D. J. 2000, BaltA, 9, 425
Sullivan, D. J. 2005, in ASP Conf. Ser. 334, 14th European Workshop on White Dwarfs, ed. D. Koester & S. Moehler (San Francisco, CA: ASP), 495
Sullivan, D. J., Metcalfe, T. S., O'Donoghue, D., et al. 2007, in ASP Conf. Ser. 372, 15th European Workshop on White Dwarfs, ed. R. Napiwotzki & M. R. Burleigh (San Francisco, CA: ASP), 629
Sullivan, D. J., Metcalfe, T. S., O'Donoghue, D., et al. 2008, MNRAS, 387, 137
Taylor, J. H., Fowler, L. A., & McCulloch, P. M. 1979, Natur, 277, 437
Thompson, S. E., & Mullally, F. 2009, JPhCS, 172, 012081
Thorsett, S. E., Arzoumanian, Z., & Taylor, J. H. 1993, ApJL, 412, L33
Unno, W., Osaki, Y., Ando, H., & Shibahashi, H. 1979, in Nonradial Oscillations of Stars (Tokyo: Univ. Tokyo Press), 330
Winget, D. E., Sullivan, D. J., Metcalfe, T. S., Kawaler, S. D., & Montgomery, M. H. 2004, ApJL, 602, L109
Wolszczan, A., & Frail, D. A. 1992, Natur, 355, 145
Wu, Y. 2001, MNRAS, 323, 248